Algebraic model of a wall acoustic impedance constructed using experimental data

B. Faverjon, Christian Soize

Algebraic model of a wall acoustic impedance constructed using an experimental data

B. Faverjon[(1)], **C. Soize**[(2)]
[(1)]Structural Dynamics and Coupled Systems Department, ONERA, BP 72, 92322 Chatillon Cedex, France
[(2)]Laboratory of Engineering Mechanics, University of Marne-La-Vallée, 77454 Marne-La-Vallée, France
e-mail:faverjon@onera.fr, soize@univ-mlv.fr

Abstract
In the context of a research devoted to the construction of a wall acoustic impedance model for a soundproofing scheme constituted of a porous medium inserted between two thin plates, an experimental data basis was carried out. In this paper, we present a probabilistic algebraic model of a wall acoustic impedance, constructed using this experimental data basis and allowing such a soundproofing scheme to be modeled. This kind of probabilistic algebraic model can be used for validating finite element model of such a soundproofing scheme whose equations are derived from the Biot theory, or for validating theoretical model, adapted to medium and high frequency ranges, deduced from Biot's equations. This probabilistic algebraic model is constructed by using the general mathematical properties of wall acoustic impedance operators (symmetry, odd and even functions with respect to the frequency, decreasing functions when frequency goes to infinity, behavior when frequency goes to zero and so onã). The parameters introduced in this probabilistic algebraic model are fitted with the experimental data basis.

1 Introduction

The modeling of a multilayer system containing poroelastic materials is very important for noise control in aircrafts, automobiles, buildings, etc. Lots of studies use numerical techniques such as the finite element method. Three-dimensional finite element numerical models have recently been developed [1,2]. An alternative to the three-dimensional finite element models is the use of an equivalent wall acoustic impedance modeling the multilayer system. In this paper, we propose a probabilistic algebraic model for such a wall acoustic impedance based on theoretical developments. The unknown parameters of this model are fitted using an experiment recently carried out at ONERA [3]. The studied multilayer system is constituted of a poroelastic material inserted between two thin plates. In a first section, the wall acoustic impedance experiment is described. The second section presents the construction of the basic algebraic model for this wall acoustic impedance constructed using general mathematical properties of wall acoustic impedance operators. In a third section, the mean values of the model parameters are fitted with experimental data basis. We then obtain the mean algebraic model. Finally, the last section deals with the construction of the probabilistic model.

2 Description of a wall acoustic impedance experiment

An experiment [3] was carried out in an anechoic room in order to measure the wall acoustic impedance of a multilayer system constituted of a three-dimensional poroelastic medium inserted between two thin plates in aluminium, denoted as P_1 and P_2 (see figure 1).

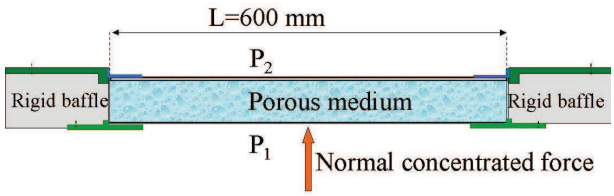

Figure 1: Description of the experiment

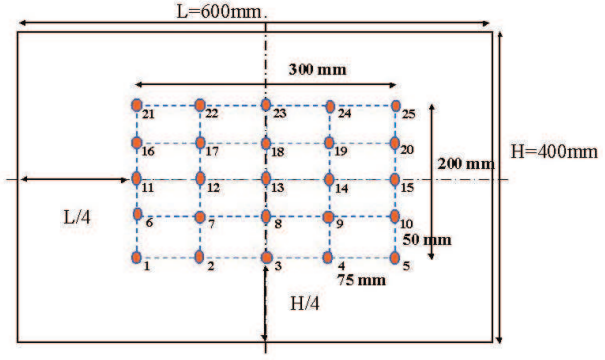

Figure 2: Position of the 25 measure points in plate P_1 and in the corresponding 25 points in plate P_2

Normal concentrated forces are successively applied to the 25 points in plate P_1 defined in figure 2. The measured responses are the normal accelerations at the 25 points in plate P_1 and at the corresponding 25 points in plate P_2. Let $\hat{F}_k^{exp}(\omega)$ be the Fourier transform of the normal concentrated force applied to the point M_k belonging to the 25 points in plate P_1. Let $\hat{V}_{jk}^{P_1\,exp}$ and $\hat{V}_{jk}^{P_2\,exp}$ be the Fourier transform of the normal velocities at the point M_j belonging to the 25 points in plate P_1 and at the corresponding point in plate P_2. The experiment consisted in identifying the 25 frequency response functions defined by

$$\hat{F}_k^{exp}(\omega) \mapsto \begin{bmatrix} \hat{V}_{1k}^{P_1\,exp}(\omega) - \hat{V}_{1k}^{P_2\,exp}(\omega) \\ . \\ . \\ . \\ . \\ . \\ \hat{V}_{Nk}^{P_1\,exp}(\omega) - \hat{V}_{Nk}^{P_2\,exp}(\omega) \end{bmatrix} , \qquad (1)$$

for k equal 1 to 25, N=25, and over the frequency band [30,1600] Hz.

3 Construction of the basic algebraic model for a wall acoustic impedance density function

3.1 Setting the problem

The theoretical problem considered introduces an applied pressure acting on plate P_1. Let $\hat{v}^{P_2}(\mathbf{x}',\omega)$ be the normal velocity to plate P_2 at the point $\mathbf{x}'$ of the middle surface S of plate P_2. Let $\hat{v}^{P_1}(\mathbf{x}',\omega)$ be the normal velocity to plate P_1 at the corresponding point $\mathbf{x}'$ (see figure 3).

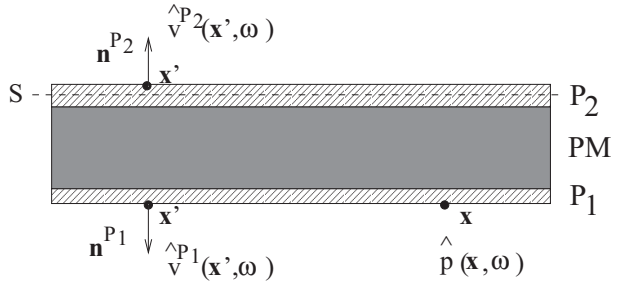

Figure 3: Frequency response function : normal velocities $\hat{v}^{P_1}(\mathbf{x}',\omega)$ on plate P_1 and $\hat{v}^{P_2}(\mathbf{x}',\omega)$ on plate P_2 when a pressure is applied to plate P_1.

3.2 Definition of the wall acoustic impedance density function

For all ω in $\mathbb{R}$, the wall acoustic impedance operator describing the acoustic insulated system is the integral operator $\mathbb{Z}(\omega)$ defined by a density function $z(\mathbf{x},\mathbf{x}',\omega)$ with complex values such that [4,5] :

$$\begin{aligned} \hat{p}(\mathbf{x},\omega) =& \{\mathbb{Z}(\omega)\,(\hat{v}^{P_1}(.,\omega) - \hat{v}^{P_2}(.,\omega))\}(\mathbf{x}) \\ =& \int_{\mathbf{x}'\in S} z(\mathbf{x},\mathbf{x}',\omega)\,(\hat{v}^{P_1}(\mathbf{x}',\omega) - \hat{v}^{P_2}(\mathbf{x}',\omega))\,dS_{\mathbf{x}'} , \end{aligned} \qquad (2)$$

in which $(\mathbf{x},\mathbf{x}') \mapsto z(\mathbf{x},\mathbf{x}',\omega)$ is called the wall acoustic impedance density function. It should be noted that operator $\mathbb{Z}(\omega)$ is defined by the complex bilinear form

$$< \mathbb{Z}(\omega)\,u, v >= \int_S \int_S z(\mathbf{x},\mathbf{x}',\omega)\,u(\mathbf{x}')\,v(\mathbf{x})\,dS_{\mathbf{x}}\,dS_{\mathbf{x}'} . \qquad (3)$$

It is assumed that the reciprocity principles can be applied. Therefore, complex operator $\mathbb{Z}(\omega)$ is symmetric and consequently, $z(\mathbf{x},\mathbf{x}',\omega)$ satisfies the following symmetry property,

$$z(\mathbf{x},\mathbf{x}',\omega) = z(\mathbf{x}',\mathbf{x},\omega) . \qquad (4)$$

Moreover, the system considered being a physical system, we have the property $\mathbb{Z}(-\omega) = \overline{\mathbb{Z}(\omega)}$ which yields

$$z(\mathbf{x},\mathbf{x}',-\omega) = \overline{z(\mathbf{x},\mathbf{x}',\omega)} , \qquad (5)$$

where $\overline{a}$ denotes the conjugate of complex number a. Introducing the real part and the imaginary part of the wall acoustic impedance density function as follows

$$z(\mathbf{x},\mathbf{x}',\omega) = z_R(\mathbf{x},\mathbf{x}',\omega) + i\,z_I(\mathbf{x},\mathbf{x}',\omega) , \qquad (6)$$

from Eqs. (4) and (5), we deduce that

$$\begin{aligned} z_R(\mathbf{x},\mathbf{x}',\omega) &= z_R(\mathbf{x}',\mathbf{x},\omega) , \\ z_I(\mathbf{x},\mathbf{x}',\omega) &= z_I(\mathbf{x}',\mathbf{x},\omega) , \end{aligned} \qquad (7)$$

$$\begin{aligned} z_R(\mathbf{x},\mathbf{x}',-\omega) &= z_R(\mathbf{x},\mathbf{x}',\omega) , \\ z_I(\mathbf{x},\mathbf{x}',-\omega) &= -z_I(\mathbf{x},\mathbf{x}',\omega) . \end{aligned} \qquad (8)$$

3.3 Local wall acoustic impedance density function

The local wall acoustic impedance density function z^{loc} is defined by

$$\hat{p}(\mathbf{x},\omega) = z^{loc}(\mathbf{x},\omega)\,(\hat{v}^{P_1}(\mathbf{x},\omega) - \hat{v}^{P_2}(\mathbf{x},\omega)) \quad , \quad \forall \mathbf{x} \in S . \qquad (9)$$

From Eqs. (2) and (9), we deduce that the local wall acoustic impedance density function is then written as

$$z(\mathbf{x},\mathbf{x}',\omega) = z^{loc}(\mathbf{x},\omega)\,\delta_0(\mathbf{x}-\mathbf{x}')\;, \tag{10}$$

in which, for all $\mathbf{x}'$ inside S, $\delta_0(\mathbf{x}-\mathbf{x}')$ is the Dirac function such as

$$\int_S \phi(\mathbf{x})\,\delta_0(\mathbf{x}-\mathbf{x}')\,dS_{\mathbf{x}} = \phi(\mathbf{x}')\;. \tag{11}$$

It should be noted that $z^{loc}(\mathbf{x},\omega)$ differs from $z(\mathbf{x},\mathbf{x}',\omega)$ by a surface element. Introducing the real part and the imaginary part of the local wall acoustic impedance density function such that

$$z^{loc}(\mathbf{x},\omega) = z_R^{loc}(\mathbf{x},\omega) + i\,z_I^{loc}(\mathbf{x},\omega)\;, \tag{12}$$

from Eq.(8), we deduce that

$$\begin{aligned} z_R^{loc}(\mathbf{x},-\omega) &= z_R^{loc}(\mathbf{x},\omega) \quad , \\ z_I^{loc}(\mathbf{x},-\omega) &= -z_I^{loc}(\mathbf{x},\omega)\;. \end{aligned} \tag{13}$$

For all $\mathbf{x}$ in S, the local wall acoustic impedance density function satisfies [4]

$$\begin{aligned} z_R^{loc}(\mathbf{x},\omega) > 0 \quad , \quad \forall\omega\in\mathbb{R}\;, \\ -\omega\,z_I^{loc}(\mathbf{x},\omega) \geq 0 \quad , \quad \forall\omega\in[-\omega_0,\omega_0] \\ \text{in which} \quad \omega_0 > 0\;, \end{aligned} \tag{14}$$

$$\lim_{\omega\to 0}(-\omega\,z_I^{loc}(\mathbf{x},\omega)) = \alpha(\mathbf{x}) \geq \alpha_{min} > 0\;, \tag{15}$$

in which α_{min} is a given real positive constant and $\mathbf{x}\mapsto\alpha(\mathbf{x})$ is a positive-valued function defined on S. Equation (15) means that

$$z_I^{loc}(\mathbf{x},\omega) \sim -\alpha(\mathbf{x})/\omega \quad \text{if} \quad \omega\to 0\;. \tag{16}$$

For all $\mathbf{x}$ in S, function $\omega\mapsto z_R^{loc}(\mathbf{x},\omega)$ is a continuous function on $\mathbb{R}$ and we have

$$\lim_{\omega\to 0}(\omega\,z_R^{loc}(\mathbf{x},\omega)) = 0\;. \tag{17}$$

From Eq.(14), we deduce that

$$z^{loc}(\mathbf{x},\omega) \neq 0 \quad , \quad \forall\mathbf{x}\in S\;, \quad \forall\omega\in\mathbb{R}\;, \tag{18}$$

and from Eqs. (15) and (17), we deduce that

$$\begin{aligned} \{i\,\omega\,z^{loc}(\mathbf{x},\omega)\}_{\omega=0} &= \{-\omega\,z_I^{loc}(\mathbf{x},\omega)\}_{\omega=0} \\ &= \alpha(\mathbf{x}) > 0\;. \end{aligned} \tag{19}$$

The real part corresponds to the dissipative part of $z^{loc}(\mathbf{x},\omega)$ (acoustic impedance resistance). The imaginary part corresponds to the conservative part of $z^{loc}(\mathbf{x},\omega)$ (acoustic impedance reactance). Let $\Delta\hat{u}(\mathbf{x},\omega) = \hat{u}^{P_1}(\mathbf{x},\omega) - \hat{u}^{P_2}(\mathbf{x},\omega)$ be the difference between the normal displacements of the two plates and let be $\Delta\hat{v}(\mathbf{x},\omega) = \hat{v}^{P_1}(\mathbf{x},\omega) - \hat{v}^{P_2}(\mathbf{x},\omega)$. We then have

$$\Delta\hat{v}(\mathbf{x},\omega) = i\,\omega\,\Delta\hat{u}(\mathbf{x},\omega)\;. \tag{20}$$

From (9) and (20), we deduce that

$$\begin{aligned} \hat{p}(\mathbf{x},\omega) =& z^{loc}(\mathbf{x},\omega)\,\Delta\hat{v}(\mathbf{x},\omega) \\ =& i\,\omega\,z^{loc}(\mathbf{x},\omega)\,\Delta\hat{u}(\mathbf{x},\omega) \\ =& [-\omega\,z_I^{loc}(\mathbf{x},\omega) + i\,\omega\,z_R^{loc}(\mathbf{x},\omega)]\,\Delta\hat{u}(\mathbf{x},\omega)\;. \end{aligned} \tag{21}$$

Figure 4 displays a typical graph [4] for functions $\omega\mapsto z_R^{loc}(\mathbf{x},\omega)$ and $\omega\mapsto z_I^{loc}(\mathbf{x},\omega)$.

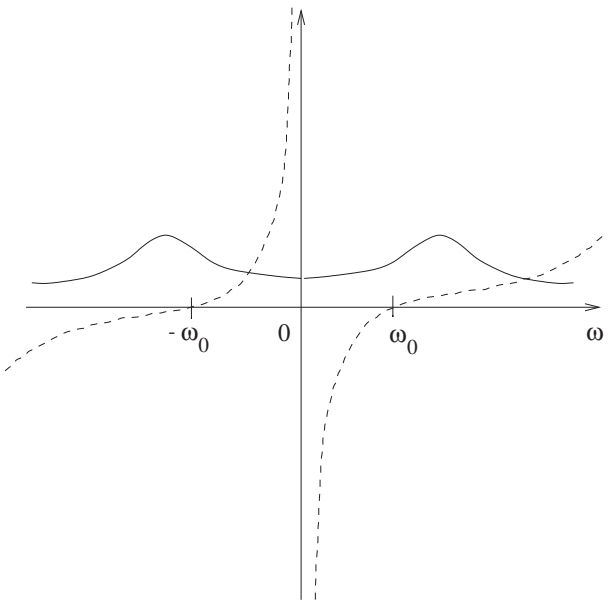

Figure 4: Acoustic impedance resistance z_R^{loc} (solid line) and acoustic impedance reactance z_I^{loc} (dash line) for a local wall acoustic impedance density function z^{loc} as a function of frequency ω.

3.4 Model for the wall acoustic impedance density function

Let $\zeta(\mathbf{x},\omega)$ defined as

$$\zeta(\mathbf{x},\omega) = z(\mathbf{x},\mathbf{x},\omega)\;. \tag{22}$$

We introduce the real part and the imaginary part of $\zeta(\mathbf{x},\omega)$,

$$\zeta(\mathbf{x},\omega) = \zeta_R(\mathbf{x},\omega) + i\,\zeta_I(\mathbf{x},\omega)\;. \tag{23}$$

As explained in Section 3.3, $z^{loc}(\mathbf{x},\omega)$ differs from $\zeta(\mathbf{x},\omega)$ by a surface element. Since $z_R^{loc}(\mathbf{x},\omega) > 0$, we then deduce that $\zeta_R(\mathbf{x},\omega) > 0$. Let $\rho_R(\mathbf{x},\mathbf{x}',\omega)$ be the function corresponding to the normalization of $z_R(\mathbf{x},\mathbf{x}',\omega)$ such as

$$\rho_R(\mathbf{x},\mathbf{x}',\omega) = \frac{z_R(\mathbf{x},\mathbf{x}',\omega)}{\sqrt{\zeta_R(\mathbf{x},\omega)\,\zeta_R(\mathbf{x}',\omega)}}\ . \qquad (24)$$

For the imaginary part, there are ω such that $\zeta_I(\mathbf{x},\omega) = 0$. Consequently, the normalization of the imaginary part is defined by

$$\rho_I(\mathbf{x},\mathbf{x}',\omega) = \frac{z_I(\mathbf{x},\mathbf{x}',\omega)}{\sqrt{|\zeta(\mathbf{x},\omega)|\,|\zeta(\mathbf{x}',\omega)|}}\ . \qquad (25)$$

We then obtain

$$z(\mathbf{x},\mathbf{x}',\omega) = \sqrt{|\zeta(\mathbf{x},\omega)|\,|\zeta(\mathbf{x}',\omega)|}\,\Big(\rho_R(\mathbf{x},\mathbf{x}',\omega) \times\sqrt{\frac{\zeta_R(\mathbf{x},\omega)}{|\zeta(\mathbf{x},\omega)|}}\,\sqrt{\frac{\zeta_R(\mathbf{x}',\omega)}{|\zeta(\mathbf{x}',\omega)|}} + i\,\rho_I(\mathbf{x},\mathbf{x}',\omega)\Big)\ . \qquad (26)$$

3.5 Basic algebraic model

A detailed analysis of the experimental data basis was carried out. For the experiment under consideration, it can be considered that (1) the wall acoustic impedance can be considered as local in space for frequencies greater than 300 Hz (the local wall acoustic impedance assumption is not verified below 300 Hz); nevertheless, below, we present the results for all the frequency band; (2) for frequencies greater than 300 Hz, the wall acoustic impedance density function can be considered as homogeneous and isotropic. Consequently, $z(\mathbf{x},\mathbf{x}',\omega)$ depends only on $||\mathbf{x}-\mathbf{x}'||$ and is rewritten as $z(||\mathbf{x}-\mathbf{x}'||,\omega)$. Therefore, $\zeta(\mathbf{x},\omega)$ does not depend on $\mathbf{x}$,

$$\zeta(\mathbf{x},\omega) = \zeta(\omega)\ . \qquad (27)$$

Equation (26) is then rewritten as

$$z(||\mathbf{x}-\mathbf{x}'||,\omega) = |\zeta(\omega)|\,\Big(\rho_R(||\mathbf{x}-\mathbf{x}'||,\omega)\,\frac{\zeta_R(\omega)}{|\zeta(\omega)|} + i\,\rho_I(||\mathbf{x}-\mathbf{x}'||,\omega)\Big)\ . \qquad (28)$$

For the function $\rho_R(||\mathbf{x}-\mathbf{x}'||,\omega)$, we propose the following algebraic model,

$$\rho_R(||\mathbf{x}-\mathbf{x}'||,\omega) = e^{-\frac{||\mathbf{x}-\mathbf{x}'||}{L_R(\omega)}}\,\cos\left(\frac{2\,\pi}{\lambda_R(\omega)}\,||\mathbf{x}-\mathbf{x}'||\right)\ , \qquad (29)$$

and for $\rho_I(||\mathbf{x}-\mathbf{x}'||,\omega)$,

$$\rho_I(||\mathbf{x}-\mathbf{x}'||,\omega) = e^{-\frac{||\mathbf{x}-\mathbf{x}'||}{L_I(\omega)}}\,\cos\Big(\frac{2\,\pi}{\lambda_I(\omega)}\,||\mathbf{x}-\mathbf{x}'|| + \phi_I(\omega)\Big)\ . \qquad (30)$$

4 Estimating the mean values of the basic algebraic model parameters using the experimental data basis

The objective is to estimate (1) the values of $\zeta_R(\omega)$, $\zeta_I(\omega)$, $|\zeta(\omega)|$ and $\phi_I(\omega)$ and (2) a mean value of basic algebraic model parameters L_R, λ_R, L_I, λ_I and ϕ_I denoted as $\underline{L}_R$, $\underline{\lambda}_R$, $\underline{L}_I$, $\underline{\lambda}_I$ and $\underline{\phi}_I$.

4.1 Estimation of $\zeta_R(\omega)$

Since experimental values of $\zeta_R(\mathbf{x}_j,\omega)$ on all 25 measured points $\mathbf{x}_j$, $j = 1$ to 25, are close together, the assumption introduced concerning the space homogeneity is satisfied. Consequently, we introduce $\zeta_R^{exp}(\omega) = \frac{1}{25}\sum_{j=1}^{25}\zeta_R(\mathbf{x}_j,\omega)$ which represents the experimental mean value. Figure 5 displays the comparison of $\zeta_R^{exp}(\omega)$ with $\zeta_R(\omega)$ over the frequency band [100,1600] Hz.

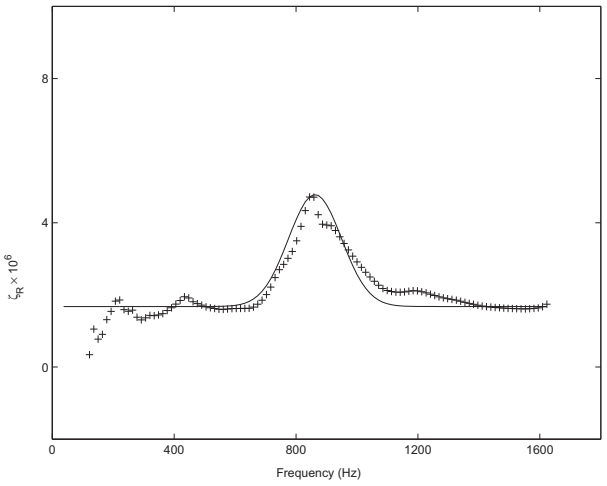

Figure 5: Graphs of $\zeta_R(\omega)$ (solid line) and of $\zeta_R^{exp}(\omega)$ (cross) over the frequency band [100,1600] Hz.

The model we propose for $\zeta_R(\omega)$ is defined by

$$\zeta_R(\omega) = \zeta_{R\,0} + (\zeta_{R\,max} - \zeta_{R\,0})\,\left(\frac{|\omega|}{\omega_{R0}}\right)^{\gamma_R} e^{-a_R\left|\frac{|\omega|}{\omega_{R0}}-1\right|^{b_R}}\ , \qquad (31)$$

in which the estimation of the parameters ζ_{R0}, $\zeta_{R\,max}$, ω_{R0}, γ_R, a_R and b_R yields

$$\begin{aligned}\zeta_{R\,0} &= 1.678\times10^6\ \text{Pa.s.m}^{-3}\ ,\\ \zeta_{R\,max} &= 4.717\times10^6\ \text{Pa.s.m}^{-3}\ ,\\ \omega_{R0} &= 5303\ \text{rad.s}^{-1}\ ,\\ \gamma_R &= 2\ ,\\ a_R &= 46\ ,\\ b_R &= 2\ .\end{aligned} \qquad (32)$$

It should be noted that the graph of $\zeta_R(\omega)$ looks like to the typical graph shown in figure 4 (solid line).

4.2 Estimation of $\zeta_I(\omega)$

Similarly, we introduce $\zeta_I^{exp}(\omega) = \frac{1}{25}\sum_{j=1}^{25}\zeta_I(\mathbf{x}_j,\omega)$ which represents the experimental mean value. Figure 6 displays the comparison of $\zeta_I^{exp}(\omega)$ with $\zeta_I(\omega)$ over the frequency band [100,1600] Hz. The model we propose for $\zeta_I(\omega)$ is defined by

$$\zeta_I(\omega) = \frac{a_I}{\omega}\left(b_I\,\omega^4 + c_I\,\omega^2 - 1 + \frac{d_I}{(\omega^2-\omega_{I0}^2)^2 + e_I\,\omega^2}\right), \tag{33}$$

in which the estimation of the parameters ω_{I0}, a_I, b_I, c_I, d_I andt e_I yields

$$\begin{aligned} \omega_{I0} &= 4.86\,10^3\ \text{rad.s}^{-1}\ , \\ a_I &= 4.7\,10^9\ , \\ b_I &= 8\,10^{-16}\ , \\ c_I &= 1\,10^{-25}\ , \\ d_I &= 1.6\,10^{14}\ , \\ e_I &= 2.4\,10^6\ . \end{aligned} \tag{34}$$

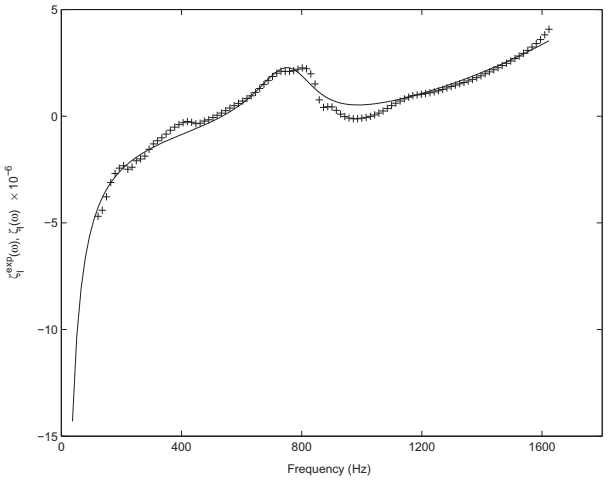

Figure 6: Graphs of $\zeta_I(\omega)$ (solid line) and of $\zeta_I^{exp}(\omega)$ (cross) over the frequency band [100,1600] Hz.

It should be noted that the graph of $\zeta_I(\omega)$ looks like to the typical graph shown in figure 4 (dashed line).

4.3 Calculation of modulus $|\zeta(\omega)|$ and experimental comparison

Using Eqs(31) to (34), modulus $|\zeta(\omega)|$ is calculated by

$$|\zeta(\omega)| = \sqrt{\zeta_R(\omega)^2 + \zeta_I(\omega)^2}\ , \tag{35}$$

and the corresponding experimental value is $|\zeta^{exp}(\omega)| = \sqrt{\zeta_R^{exp}(\omega)^2 + \zeta_I^{exp}(\omega)^2}$. Figure 7 shows the comparison of $|\zeta^{exp}(\omega)|$ with $|\zeta(\omega)|$ defined by Eq.(35) over the frequency band [100,1600] Hz.

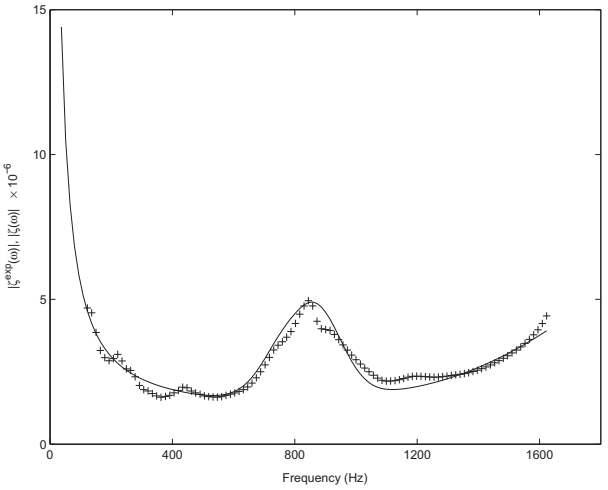

Figure 7: Graphs of $|\zeta(\omega)|$ (solid line) and of $|\zeta^{exp}(\omega)|$ (cross) over the frequency band [100,1600] Hz.

4.4 Calculation of $\phi_I(\omega)$ and experimental comparison

Phase $\phi_I(\omega)$ is deduced from Eqs.(25) and (30) (take $\mathbf{x} = \mathbf{x}'$) and is written as

$$\cos(\phi_I(\omega)) = \frac{\zeta_I(\omega)}{|\zeta(\omega)|}\ . \tag{36}$$

The correponding experimental value is such that $\cos(\phi_I^{exp}(\omega)) = \frac{\zeta_I^{exp}(\omega)}{|\zeta^{exp}(\omega)|}$. Figure 8 shows the comparison of $\phi_I^{exp}(\omega)$ with $\phi_I(\omega)$ defined by Eq.(36) over the frequency band [100,1600] Hz.

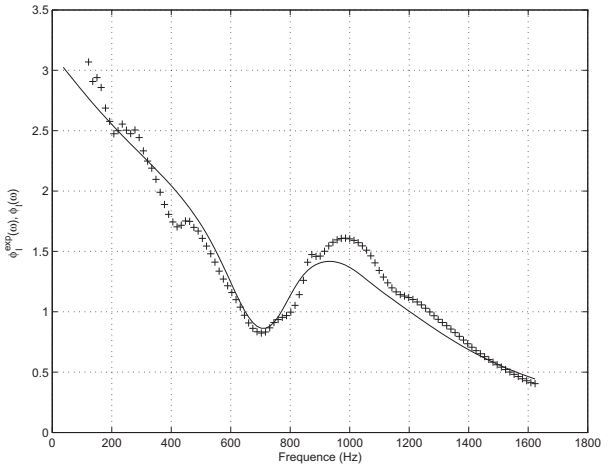

Figure 8: Graphs of $\phi_I(\omega)$ (solid line) and $\phi_I^{exp}(\omega)$ (cross) over the frequency band [100,1600] Hz

4.5 Fitting the algebraic model of $\rho_R(||\mathbf{x}-\mathbf{x}'||,\omega)$

The algebraic model proposed for $\rho_R(||\mathbf{x}-\mathbf{x}'||,\omega)$ is defined by Eq.(29). Many analyses were conducted to fit the experimental data basis with this algebraic model. The conclusions were that the best fitting is obtained when $L_R(\omega)$ and $\lambda_R(\omega)$ are taken as constants independant of ω. We then rewrite the algebraic model as

$$\rho_R(||\mathbf{x}-\mathbf{x}'||) = e^{-\frac{||\mathbf{x}-\mathbf{x}'||}{\underline{L}_R}} \cos\left(\frac{2\,\pi}{\underline{\lambda}_R}\,||\mathbf{x}-\mathbf{x}'||\right) , \quad (37)$$

in which $\underline{L}_R$ and $\underline{\lambda}_R$ are independant of ω. From the fitting, we obtain the following values

$$\begin{aligned} \underline{L}_R &= 0.0664\,, \\ \underline{\lambda}_R &= 0.0771\,. \end{aligned} \quad (38)$$

Consequently, concerning the experimental data, we introduce the function $\eta \mapsto \underline{\rho}_R^{exp}(\eta) = \frac{1}{|\mathcal{B}|} \times \int_{\mathcal{B}} \rho_R^{exp}(\eta,\omega)\,d\omega$ in which $\mathcal{B}$ is the frequency band and $\eta = ||\mathbf{x}-\mathbf{x}'||$. Figure 9 shows the graph of $\eta \mapsto \rho_R(\eta)$ (solide line) and the graph of $\eta \mapsto \underline{\rho}_R^{exp}(\eta)$ (cross symbols).

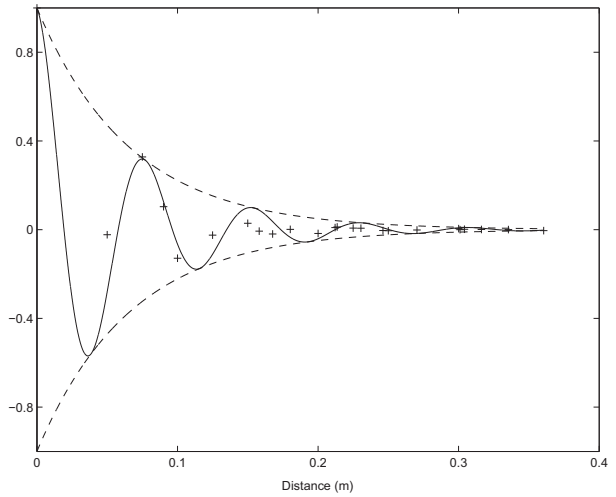

Figure 9: Graphs of the function $\eta \mapsto \rho_R(\eta)$ with $\eta = ||\mathbf{x}-\mathbf{x}'||$ the distance (solid line) and of its envelope (dash line). Graph of the function $\eta \mapsto \underline{\rho}_R^{exp}(\eta)$ (cross symbols)

Figure 10 shows that the assumption introduced concerning the independance of $\underline{L}_R$ and $\underline{\lambda}_R$ with the frequency is acceptable taking into account that the final model is a probabilistic model. In figure 10, the dotted lines correspond to the graphs $\omega \mapsto \rho_R^{exp}(\eta,\omega)$ for $\eta = 0.075$ m (in the experimental data basis, there are several couples of points $(\mathbf{x},\mathbf{x}')$ having the same distance $\eta = ||\mathbf{x}-\mathbf{x}'||$). For this value of η, the solid line represents $\rho_R(\eta)$ given by Eq.(37) with Eq.(38).

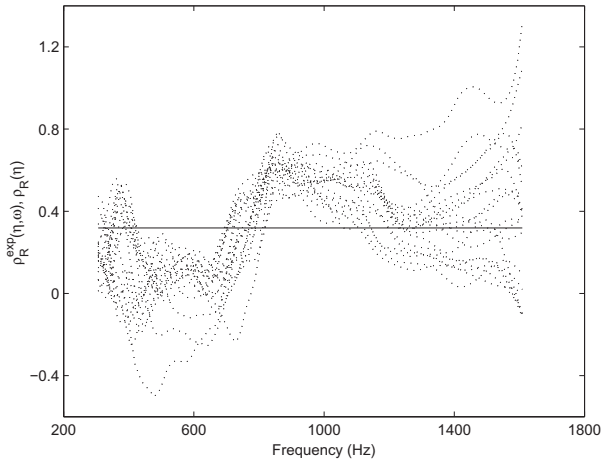

Figure 10: Graphs of the function $\omega \mapsto \rho_R^{exp}(\eta,\omega)$ (dotted lines) and graph of the function $\omega \mapsto \rho_R(\eta)$ (solid line) for $\eta = 0.075$ m

4.6 Expression of the parameters of the model of $\rho_I(\mathbf{x}-\mathbf{x}',\omega)$

The algebraic model proposed for $\rho_I(||\mathbf{x}-\mathbf{x}'||,\omega)$ is given by Eq.(30). Similarly, $L_I(\omega)$ and $\lambda_I(\omega)$ are taken as constants independant of ω. We then rewrite the algebraic model as

$$\rho_I(\eta) = e^{-\frac{\eta}{\underline{L}_I}} \cos\left(\frac{2\,\pi}{\underline{\lambda}_I}\,\eta + \underline{\phi}_I\right) , \quad (39)$$

in which $\underline{L}_I$ and $\underline{\lambda}_I$ are independant of ω and in which $\underline{\phi}_I$ is the average value such as $\underline{\phi}_I = \frac{1}{|\mathcal{B}|}\int_{\mathcal{B}} \phi_I(\omega)\,d\omega$. The average value $\underline{\phi}_I$ is given by

$$\underline{\phi}_I = 1.1697 \text{ rad}\,. \quad (40)$$

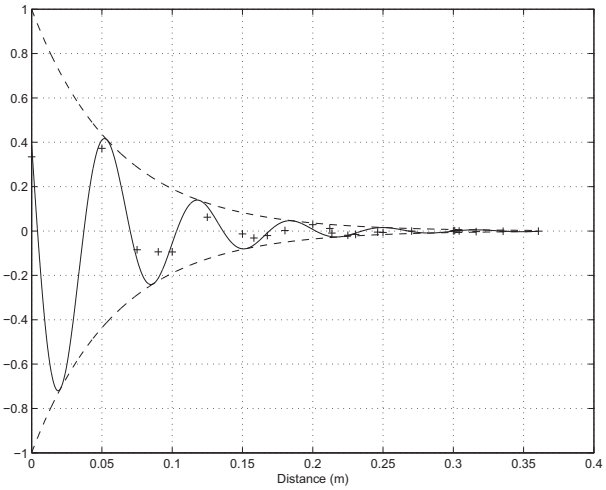

Figure 11: Graphs of the function $\eta \mapsto \rho_I(\eta)$ with $\eta = ||\mathbf{x}-\mathbf{x}'||$ the distance (solid line) and of its envelope (dash line). Graph of the function $\eta \mapsto \underline{\rho}_I^{exp}(\eta)$ (cross symbols)

From the fitting, we obtain the following values

$$\underline{L}_I = 0.0603 \, ,$$
$$\underline{\lambda}_I = 0.0660 \, . \qquad (41)$$

Concerning the experimental data, we introduce the function $\eta \mapsto \underline{\rho}_I^{exp}(\eta) = \frac{1}{|\mathcal{B}|} \int_{\mathcal{B}} \rho_I^{exp}(\eta, \omega) \, d\omega$. Figure 11 shows the graph of $\eta \mapsto \rho_I(\eta)$ (solide line) and the graph of $\eta \mapsto \underline{\rho}_I^{exp}(\eta)$ (cross symbols).
Figure 12 shows that the assumption introduced concerning the independance of $\underline{L}_I$ and $\underline{\lambda}_I$ with the frequency is acceptable taking into account that the final model is a probabilistic model. In figure 12, the dotted lines correspond to the graphs $\omega \mapsto \rho_I^{exp}(\eta, \omega)$ for $\eta = 0.075$ m. For this value of η, the solid line represents $\rho_I(\eta)$ given by Eq.(39) with Eqs.(40) and (41).

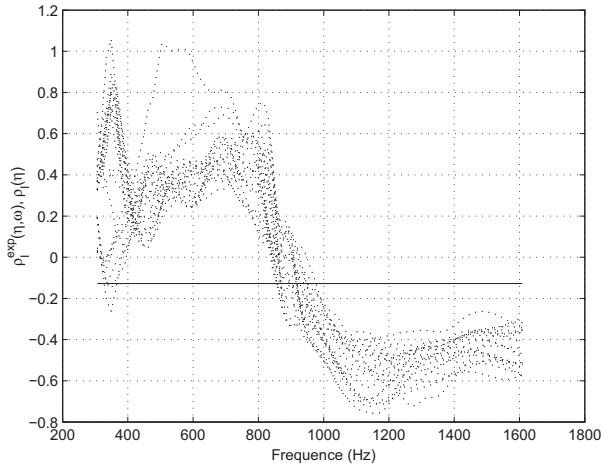

Figure 12: Graphs of the function $\omega \mapsto \rho_I^{exp}(\eta, \omega)$ (dotted lines) and graph of the function $\omega \mapsto \rho_I(\eta)$ (solid line) for $\eta = 0.075$ m

5 Construction of a random model for $\rho_R(\eta)$ and $\rho_I(\eta)$

A detailed analysis has been carried out in order to define the parameters of the basic algebraic model which had to be modeled by a random variable. The retained model is the basic algebraic model in which ζ_R and $|\zeta|$ are modeled by the mean values estimated in sections 4.1 and 4.3, L_R and L_I are modeled by $\underline{L}_R$ and $\underline{L}_I$ estimated in sections 4.5 and 4.6 and where λ_R, λ_I and ϕ_I are modeled by mutually independent random variables Λ_R, Λ_I and Φ_I respectively, independent of frequency ω. By construction, the mean values of these three random variables are mean values $\underline{\lambda}_R$, $\underline{\lambda}_I$ and $\underline{\phi}_I$ estimated in sections 4.5 and 4.6.

5.1 Estimating the probability distributions of the random parameters

Random variables Λ_R and Λ_I are positive-valued random variables and Φ_I is a random variable with values in $[0, 2\,\pi]$. We choose the maximum entropy distribution [6] for each random variable Λ_R, Λ_I and Φ_I. First, consider the case of Λ_R (respectively Λ_I). The entropy $\mathcal{S}$ of an absolutely continuous distribution with probability density function $p_{\Lambda_R}(\lambda)$ (resp. $p_{\Lambda_I}(\lambda)$) is defined by

$$\mathcal{S}(p_{\Lambda_R}(\lambda)) = -\int_{\mathbb{R}^+} p_{\Lambda_R}(\lambda) \, ln(p_{\Lambda_R}(\lambda)) \, d\lambda \, , \qquad (42)$$

$$\Big(\text{resp. } \mathcal{S}(p_{\Lambda_I}(\lambda)) = -\int_{\mathbb{R}^+} p_{\Lambda_I}(\lambda) \, ln(p_{\Lambda_I}(\lambda)) \, d\lambda\Big) . \qquad (43)$$

The maximization of $\mathcal{S}$, subject to the moment constraints,

$$\int_{\mathbb{R}_+} \lambda^r \, p_{\Lambda_R}(\lambda) \, d\lambda = m_r^R \quad , \quad r = 0, 1, 2 \, , \qquad (44)$$

$$\Big(\text{resp. } \int_{\mathbb{R}_+} \lambda^r \, p_{\Lambda_I}(\lambda) \, d\lambda = m_r^I \quad , \quad r = 0, 1, 2\Big) , \qquad (45)$$

leads to

$$p_{\Lambda_R}(\lambda) = \mathbb{1}_{\mathbb{R}^+}(\lambda) \, C_0^R \, e^{-\mu_1^R \, \lambda - \mu_2^R \, \lambda^2} \, , \qquad (46)$$

$$\Big(\text{resp. } \quad p_{\Lambda_I}(\lambda) = \mathbb{1}_{\mathbb{R}^+}(\lambda) \, C_0^I \, e^{-\mu_1^I \, \lambda - \mu_2^I \, \lambda^2}\Big) \, , \qquad (47)$$

in which $C_0^R > 0$, μ_1^R and $\mu_2^R > 0$ (resp. $C_0^I > 0$, μ_1^I and $\mu_2^I > 0$) have to be chosen such that the moment constraints be satisfied. Moments m_r^R, $r = 0, 1, 2$, (resp. m_r^I, $r = 0, 1, 2$) are defined by

$$m_0^R = 1 \ , \ m_1^R = \underline{\lambda}_R \ , \ m_2^R = {\underline{\lambda}_R}^2 + \sigma_{\Lambda_R}^2 \, , \qquad (48)$$

$$\Big(\text{resp. } m_0^I = 1 \ , \ m_1^I = \underline{\lambda}_I \ , \ m_2^I = {\underline{\lambda}_I}^2 + \sigma_{\Lambda_I}^2\Big) , \qquad (49)$$

in which $\underline{\lambda}_R$ (resp. $\underline{\lambda}_I$) is the mean value and $\sigma_{\Lambda_R}^2$ (resp. $\sigma_{\Lambda_I}^2$) is the variance such that

$$E\{\Lambda_R\} = \underline{\lambda}_R \, ,$$
$$\sigma_{\Lambda_R}^2 = E\{(\Lambda_R - \underline{\lambda}_R)^2\} = E\{\Lambda_R^2\} - {\underline{\lambda}_R}^2 \, , \qquad (50)$$

$$\Big(\text{resp. } \quad E\{\Lambda_I\} = \underline{\lambda}_I \, ,$$
$$\sigma_{\Lambda_I}^2 = E\{(\Lambda_I - \underline{\lambda}_I)^2\} = E\{\Lambda_I^2\} - {\underline{\lambda}_I}^2\Big) . \qquad (51)$$

Using the experimental data basis for estimating the parameters yields

$$\sigma_{\Lambda_R} = 0.0324 \quad , \quad C_0^R = 0.926 > 0 \, ,$$
$$\mu_1^R = -67.377 \quad , \quad \mu_2^R = 442.809 > 0 \, , \qquad (52)$$

$\Big($resp.

$$\sigma_{\Lambda_I} = 0.0274 \quad , \quad C_0^I = 1.012 > 0 \, ,$$
$$\mu_1^I = -81.157 \quad , \quad \mu_2^I = 622.792 > 0\Big) \, . \qquad (53)$$

For random variable Φ_I, the entropy $\mathcal{S}$ is written as

$$S(p_{\Phi_I}(\phi)) = -\int_0^{2\,\pi} p_{\Phi_I}(\phi)\, ln(p_{\Phi_I}(\phi))\, d\phi \, , \qquad (54)$$

with probability density function $p_{\Phi_I}(\phi)$ defined by

$$p_{\Phi_I}(\phi) = \mathbb{1}_{[0,2\,\pi]}(\phi)\, C_0^\phi \, e^{-\mu_1^\phi \, \phi - \mu_2^\phi \, \phi^2} \, , \qquad (55)$$

in which C_0^ϕ, μ_1^ϕ and μ_2^ϕ have to be chosen such that

$$\int_0^{2\,\pi} \phi^r \, p_{\Phi_I}(\phi)\, d\phi = m_r^\phi \quad , \quad r = 0, 1, 2 \, . \qquad (56)$$

Moments m_r^ϕ, $r = 0$, 1, 2, are defined by

$$m_0^\phi = 1 \ , \ m_1^\phi = \underline{\phi}_I \ , \ m_2^\phi = \underline{\phi}_I{}^2 + \sigma_{\Phi_I}^2 \, , \qquad (57)$$

in which $\underline{\phi}_I$ is the mean value given by Eq.(40) and $\sigma_{\Phi_I}^2$ is the variance such that

$$E\{\Phi_I\} = \underline{\phi}_I \, ,$$
$$\sigma_{\Phi_I}^2 = E\{(\Phi_I - \underline{\phi}_I)^2\} = E\{\Phi_I^2\} - \underline{\phi}_I{}^2 \, . \qquad (58)$$

Using the experimental data basis for estimating the parameters yields

$$\sigma_{\Phi_I} = 0.3745 \text{ rad} \quad , \quad C_0^\phi = 10.776$$
$$\mu_1^\phi = 11.124 \quad , \quad \mu_2^\phi = -1.623 \, . \qquad (59)$$

5.2 Construction of the probabilistic algebraic model for $\rho_R(\eta)$

From the basic algebraic model and from the hypotheses introduced at the beginning of Section 5, the real-valued random variable $\rho_R(\eta)$ is defined by

$$\rho_R(\eta) = e^{-\frac{\eta}{L_R}} \, \cos\left(\frac{2\,\pi}{\Lambda_R}\,\eta\right) \, . \qquad (60)$$

For a fixed value η of the distance, the confidence region of $\rho_R(\eta)$, corresponding to a given probability level P_c, is defined by the upper envelope $\rho_R^+(\eta)$ and the lower envelope $\rho_R^-(\eta)$ such that

$$\mathcal{P}(\rho_R^-(\eta) < \rho_R(\eta) \leq \rho_R^+(\eta)) \geq P_c \, , \qquad (61)$$

in which

$$\rho_R^-(\eta) = 2\, E\{\rho_R(\eta)\} - \rho_R^+(\eta) \, . \qquad (62)$$

The mean value of random variable $\rho_R(\eta)$ and its variance are such that

$$E\{\rho_R(\eta)\} = \int_0^{+\infty} p_{\Lambda_R}(\lambda)\, e^{-\frac{\eta}{L_R}} \, \cos\left(\frac{2\,\pi}{\lambda}\,\eta\right) \, d\lambda \, ,$$
$$\sigma_{\rho_R}^2(\eta) = E\{\rho_R(\eta)^2\} - (E\{\rho_R(\eta)\})^2 \quad . \qquad (63)$$

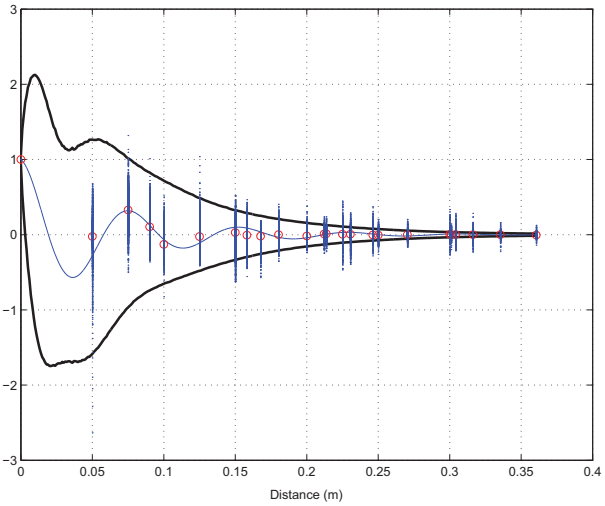

Figure 13: Confidence region of the random algebraic model $\eta \mapsto \rho_R(\eta)$, defined by the upper envelope $\eta \mapsto \rho_R^+(\eta)$ (upper thick solid line) and the lower envelope $\eta \mapsto \rho_R^-(\eta)$ (lower thick solid line). The solid line represents the graph of the mean algebraic model $\eta \mapsto \rho_R(\eta)$ defined by (37) and (38). The dot symbols (appearing as vertical solid lines for each value of distance η) correspond to the experimental data. The circle symbols correspond to the mean value of these experimental data

The upper envelope is constructed using Tchebychev's inequality [7] for a real-valued centered random variable X,

$$\mathcal{P}(|X| \geq \epsilon) \leq \frac{E\{|X|^2\}}{\epsilon^2} \, . \qquad (64)$$

We then have

$$\mathcal{P}\Big(|\rho_R(\eta) - E\{\rho_R(\eta)\}| \geq \epsilon_R(\eta)\Big) \leq \frac{E\{|\rho_R(\eta) - E\{\rho_R(\eta)\}|^2\}}{\epsilon_R^2(\eta)} \, . \qquad (65)$$

Using Eq.(63) yields

$$\mathcal{P}\Big(|\rho_R(\eta) - E\{\rho_R(\eta)\}| \geq \epsilon_R(\eta)\Big) \leq \frac{\sigma_{\rho_R}^2(\eta)}{\epsilon_R^2(\eta)} \, , \qquad (66)$$

and consequently,

$$\mathcal{P}\Big(|\rho_R(\eta) - E\{\rho_R(\eta)\}| \leq \epsilon_R(\eta)\Big) \geq P_c \, , \qquad (67)$$

in which $P_c = 1 - \frac{\sigma^2_{\rho_R}(\eta)}{\epsilon^2_R(\eta)}$. Probability level P_c being fixed, we obtain

$$\epsilon_R(\eta) = \frac{\sigma_{\rho_R}(\eta)}{\sqrt{1-P_c}} \, . \tag{68}$$

Equation (67) is rewritten as

$$\mathcal{P}\Big(-\epsilon_R(\eta) + E\{\rho_R(\eta)\} \leq \rho_R(\eta) \leq \epsilon_R(\eta) + E\{\rho_R(\eta)\}\Big) \geq P_c \, . \tag{69}$$

Comparing Eq.(69) with Eq.(61) yields

$$\rho^+_R(\eta) = E\{\rho_R(\eta)\} + \epsilon_R(\eta) \, , \tag{70}$$

$$\rho^-_R(\eta) = E\{\rho_R(\eta)\} - \epsilon_R(\eta) \, . \tag{71}$$

The confidence region corresponding to a probability level equal to 0.95 is shown in figure 13.

5.3 Construction of the probabilistic algebraic model for $\rho_I(\eta)$

Operating as in Section 5.2, the real-valued random variable $\rho_I(\eta)$ is defined by

$$\rho_I(\eta) = e^{-\frac{\eta}{L_I}} \cos\left(\frac{2\,\pi}{\Lambda_I}\,\eta + \Phi_I\right) \, . \tag{72}$$

The confidence region of $\rho_I(\eta)$ is defined by

$$\mathcal{P}(\rho^-_I(\eta) \leq \rho_I(\eta) \leq \rho^+_I(\eta)) \geq P_c \, , \tag{73}$$

in which the upper envelope is written as

$$\rho^+_I(\eta) = E\{\rho_I(\eta)\} + \epsilon_I(\eta) \, , \tag{74}$$

and the lower envelope is written as

$$\rho^-_I(\eta) = E\{\rho_I(\eta)\} - \epsilon_I(\eta) \, , \tag{75}$$

in which $\epsilon_I(\eta)$ is such that

$$\epsilon_I(\eta) = \frac{\sigma_{\rho_I}(\eta)}{\sqrt{1-P_c}} \, . \tag{76}$$

The mean value of random variable $\rho_I(\eta)$ and its variance are such that

$$E\{\rho_I(\eta)\} = \int_0^{+\infty} \int_0^{2\,\pi} p_{\Lambda_I}(\lambda)\, p_{\Phi_I}(\phi)\, e^{-\frac{\eta}{L_I}} \times \cos\left(\frac{2\,\pi}{\lambda}\,\eta + \phi\right) d\lambda\, d\phi$$

$$\sigma^2_{\rho_I}(\eta) = E\{\rho_I(\eta)^2\} - (E\{\rho_I(\eta)\})^2 \, . \tag{77}$$

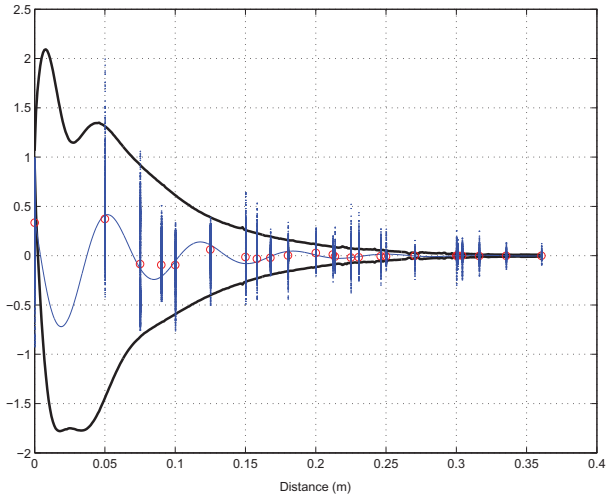

Figure 14: Confidence region of the random algebraic model $\eta \mapsto \rho_I(\eta)$, defined by the upper envelope $\eta \mapsto \rho^+_I(\eta)$ (upper thick solid line) and the lower envelope $\eta \mapsto \rho^-_I(\eta)$ (lower thick solid line). The solid line represents the graph of the mean algebraic model $\eta \mapsto \rho_I(\eta)$ defined by Eqs.(39) to (41). The dot symbols (appearing as vertical solid lines for each value of distance η) correspond to the experimental data. The circle symbols correspond to the mean value of these experimental data

The confidence region corresponding to a probability level equal to 0.95 is shown in figure 14.

6 Conclusion

In this paper, we have presented a probabilistic algebraic model for a wall acoustic impedance modeling a multilayer system constituted of a poroelastic material and of two thin plates. This construction is based on theoretical developments and on an experimental data basis allowing the introduced hypotheses to be verified and allowing the unknown parameters of the probabilistic algebraic model to be fitted. The probabilistic algebraic model is constituted of the mean algebraic model and of the probability distribution of the random model parameters. This work has been performed in order to construct an algebraic representation of a large experimental data basis, using a small number of parameters for the algebraic model.

References

[1] R. Panneton and N. Atalla, *An efficient finite element scheme for solving the three-dimensional poroelasticity problem in acoustics*, Journal of Acoustical Society of America, Vol 101, Acoustical Society of America (1996), pp.3287-3298.

[2] N. Atalla, R. Panneton and P. Debergue, *A mixed displacement-pressure formulation for poroelastic materials*, Journal of Acoustical Society of America, Vol 104, Acoustical Society of America (1998), pp.1444-1452.

[3] L. Guillaumie, *Wall acoustic impedance. Experimental identification*, ONERA report, n0 RTS 2/03239 DDSS, France (2001) (in french).

[4] R. Ohayon, C. Soize, *Structural Acoustics and Vibration*, Academic Press, San Diego (1998).

[5] A. D. Pierce, *Acoustics : An Introduction to its Physical Principles and Applications*, Acoustical Society of America Publications on Acoustics, Woodbury, New York (originally published in 1981, McGrawHill, New York) (1989).

[6] J. N. Kapur, H. K. Kesavan, *Entropy Optimization Principles with Applications*, Academic Press, San Diego (1992).

[7] M. Métivier, *Notions Fondamentales de la Théorie des Probabilités*, Dunod (1979).